Science Advances
AAAS

Supplementary Materials for

Distinct impacts of major El Niño events on Arctic temperatures due to differences in eastern tropical Pacific sea surface temperatures

Hyein Jeong, Hyo-Seok Park*, Malte F. Stuecker, Sang-Wook Yeh

*Corresponding author. Email: hspark1@gmail.com

Published 26 January 2022, *Sci. Adv.* **8**, eabl8278 (2022)
DOI: 10.1126/sciadv.abl8278

This PDF file includes:

Supplementary Text
Figs. S1 to S10
Tables S1 to S3
References

Supplementary Text

Dynamical warming

To explore the contribution of Arctic surface air temperature changes, we adopt the thermodynamic energy equation in pressure coordinates (*54*) which can be written as,

$$0 = \frac{\partial T}{\partial t} \approx \gamma T = -V_h \cdot \nabla_h T + S_p \omega + Q$$

$$S_p = -\frac{T}{\theta}\frac{\partial \theta}{\partial p},$$

where T is the temperature, t is the time, γ is the radiative relaxation time scale, V_h is the horizontal velocity vector, ∇_h is the horizontal gradient operator. The first term on the right-hand side is the horizonal temperature advection. S_p is a static stability parameter, θ is the potential temperature, p is the pressure, and ω is the vertical p velocity. The second term accounts for adiabatic warming (downward motion) or cooling (upward motion). The third term, Q represents the remaining diabatic heating contribution including latent heating, infrared radiation (IR) warming by clouds, and surface heat fluxes. We compare the relative contribution of above three terms to account for the surface air temperature changes in the Arctic.

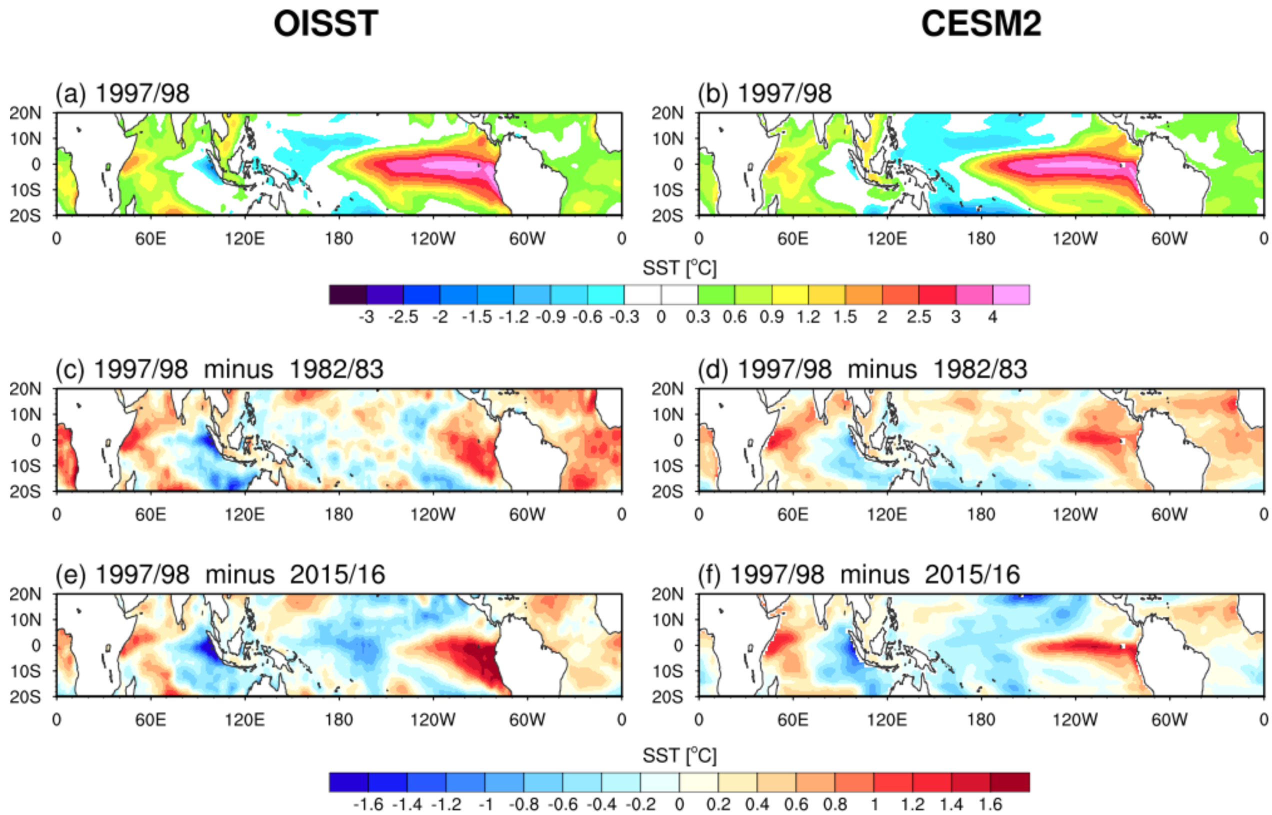

Fig. S1. Spatial differences of the tropical SST anomalies for major El Niño events. SST (shading; °C) anomalies during 1997/98 DJFM from **(a)** OISST and **(b)** the ensemble-mean of the CESM2 pacemaker simulation. Difference of SSTA between 1997/98 and 1982/83 from **(c)** OISST and **(d)** CESM2 simulation. **(e, f)** Same as **(c, d)** but 2015/16.

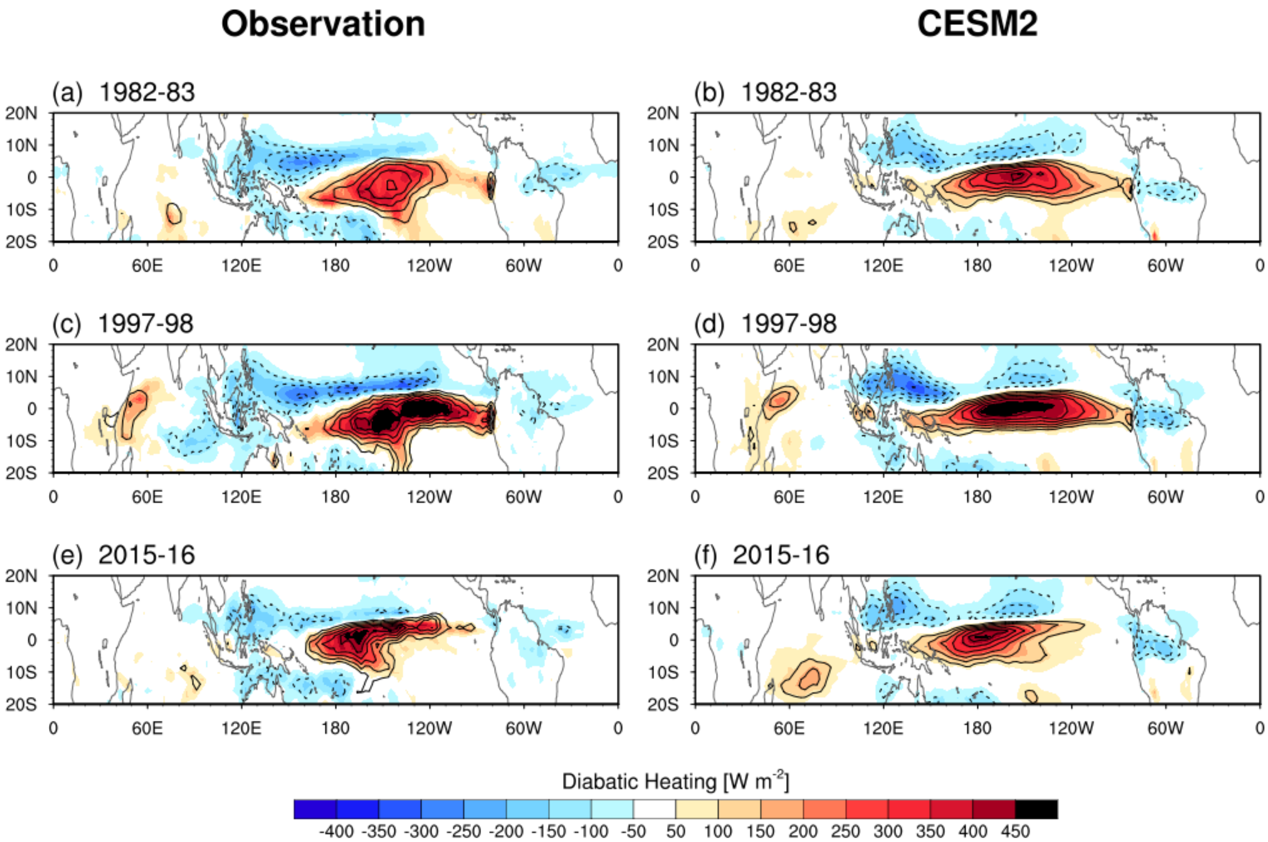

Fig. S2. Anomalous diabatic heating and precipitation in observations/reanalysis and the CESM2 pacemaker experiments. Vertically integrated diabatic heating (Shading; W m^{-2}) from 1000 hPa through 200 hPa and precipitation anomalies (contours; 2 mm/day interval) from **(left; a, c, d)** ERA5 reanalysis and GPCP, respectively, and **(right: b, d, f)** ensemble mean of the CESM2 simualtions for **(top)** 1982/83 DJFM, **(middle)** 1997/98 DJFM, and **(bottom)** 2015/16 DJFM.

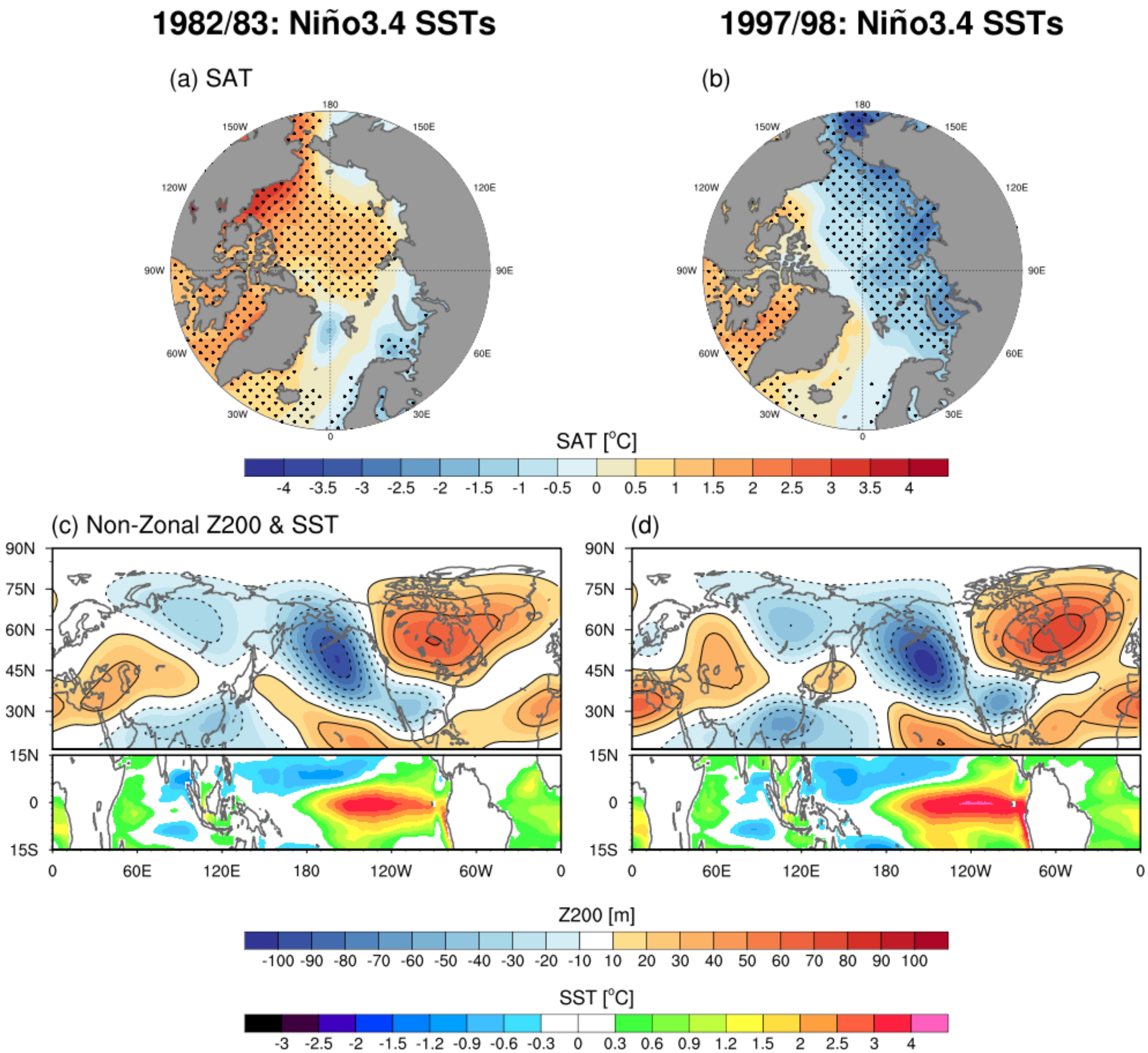

Fig. S3. Impacts of Niño3.4 SST anomalies on the Northern Hemisphere extratropics. (a, b) Surface air temperature (°C) anomalies over the Arctic Ocean and **(c, d)** tropical (15°S-15°N) SST anomalies (bottom panels; °C) and extratropical (15°N-90°N) non-zonal component of 200 hPa geopotential height anomalies (top panels; m) during boreal winter (DJFM) of **(a, c)** 1982/83 and **(b, d)** 1997/98 from CESM2 pacemaker simulation, in which Niño3.4 SST anomalies are restored. Statistically significant values ($p<0.05$) are stippled in **(a, b)**.

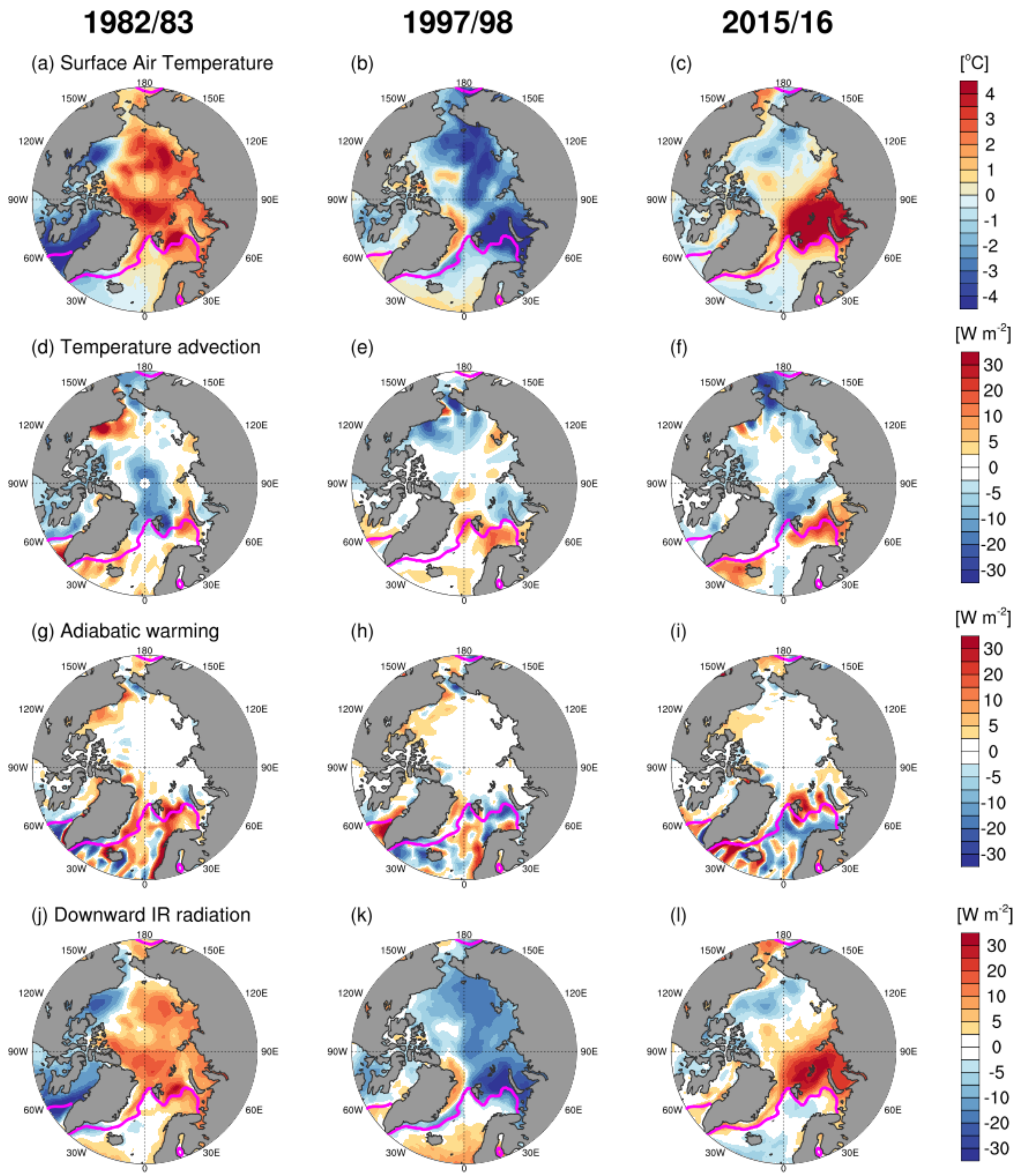

Fig. S4. Attribution of changes in the Arctic SAT in ERA5. (a, b, c) Anomalous surface air temperature (°C), verically integrated **(d, e, f)** horizontal temperature advection (W m^{-2}) and **(g, h, i)** adiabatic warming (W m^{-2}) from 1000 hPa through 850 hPa, and **(j, k, l)** downward infrared radiation (IR; W m^{-2}) from ERA5 reanalysis during (left; **a, d, g, j**) 1982/83, (middle; **b, e, h, k**) 1997/98, and (right; **c, f, i, l**) 2015/16 DJFM. Solid pink lines denote the climatological sea ice edges that correspond to 15% of sea ice concentration in observation.

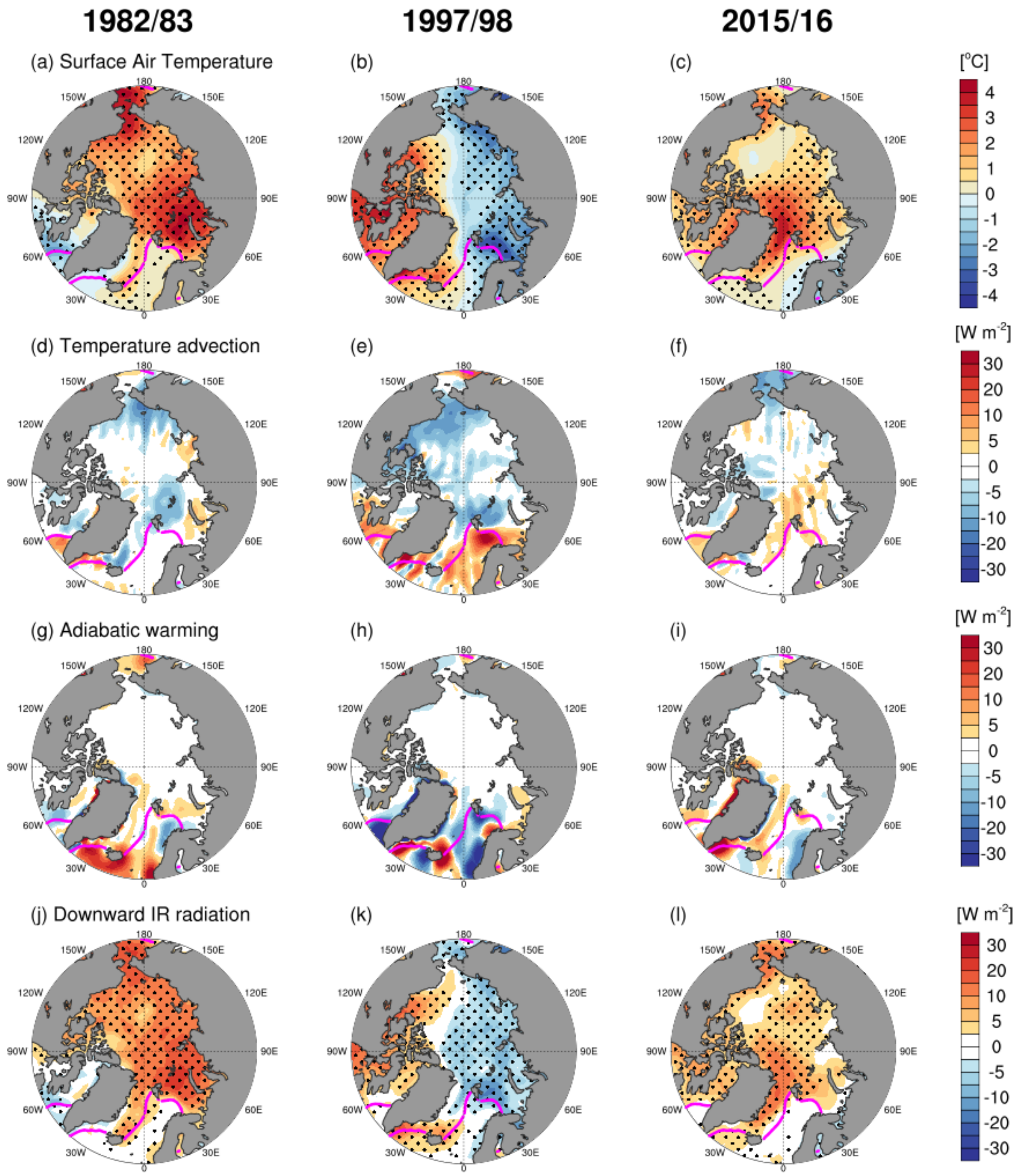

Fig. S5. Attribution of changes in the Arctic SAT in CESM2 simulation. (a, b, c) Anomalous surface air temperature (°C), verically integrated **(d, e, f)** horizontal temperature advection (W m^{-2}) and **(g, h, i)** adiabatic warming (W m^{-2}) from 1000 hPa through 850 hPa, and **(j, k, l)** downward infrared radiation (IR; W m^{-2}) from CESM2 ensemble-mean simulation during (left; **a, d, g, j**) 1982/83, (middle; **b, e, h, k**) 1997/98, and (right; **c, f, i, l**) 2015/16 DJFM. Statistically significant values ($p<0.05$) are stippled in (**a, b, c, j, k, l**). Solid pink lines denote the sea ice edges that correspond to 15% of sea ice concentration in the CESM2 control simulation.

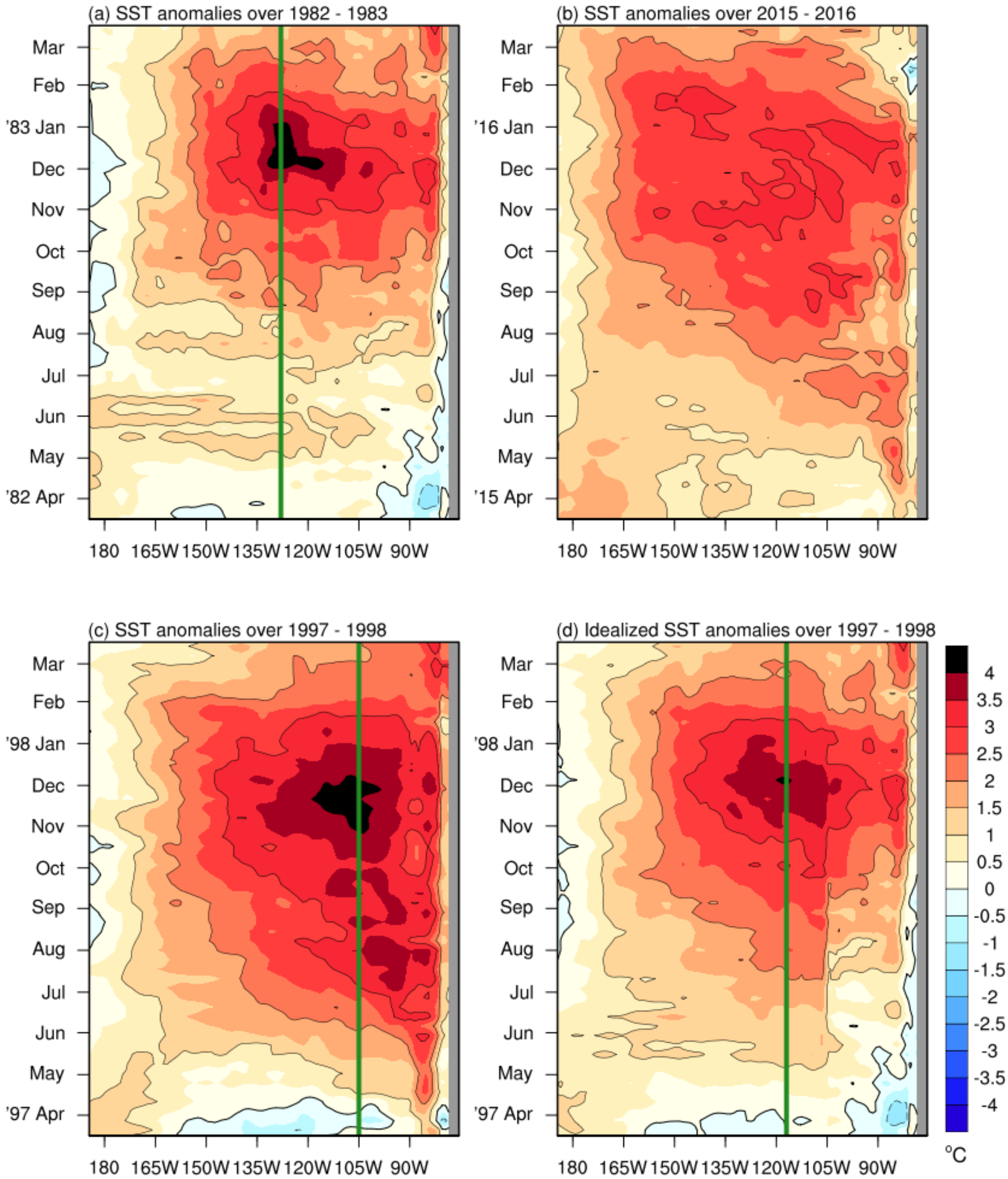

Fig. S6. Hovmöller plots of the equatorial eastern Pacific SST anomalies. Hovmöller (Longitude-Time) diagrams of observed weekly SST anomalies, averaged over 5°S to 5°N, for **(a)** 1982/83, **(b)** 2015/16, and **(c)** 1997/98 across the equatorial Pacific Ocean, from 170°E to 80°W. **(d)** Same as **(c)** except for the SST anomalies in the 'dEP' experiment.

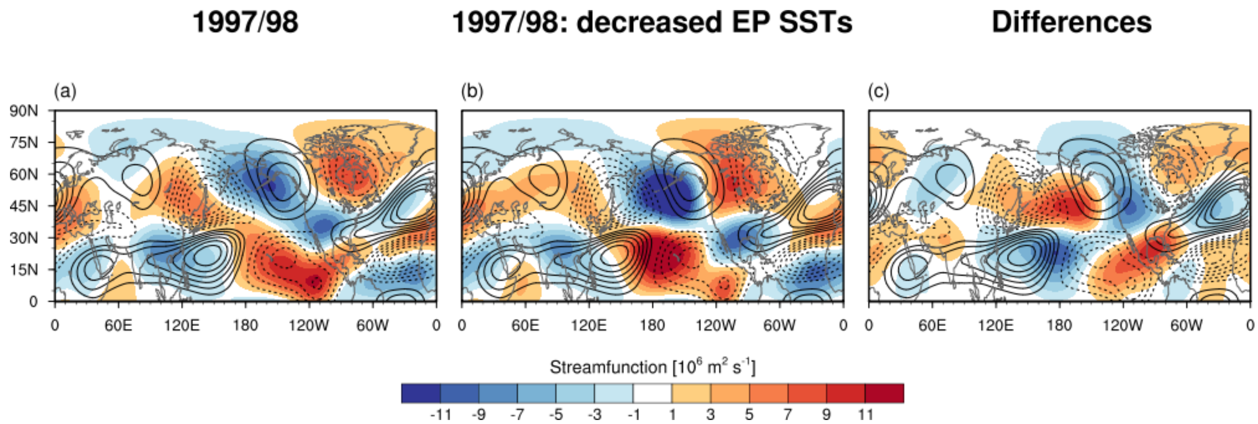

Fig. S7. Impacts of EP SSTs on extratropical stationary waves. 300 hPa eddy (i.e., zonally asymmetric) streamfunction anomalies (color shading; 10^6 m^2s^{-1}) with the climatological eddy streamfunction (contours), where solid contours indicate positive values and dashed contours negative values (contour interval is 3 x 10^6 m^2s^{-1} and the zero contour is omitted) during the winter of 1997/98 from **(a)** ENSO pacemaker simulation, **(b)** “dEP” simulation, and **(c)** their difference.

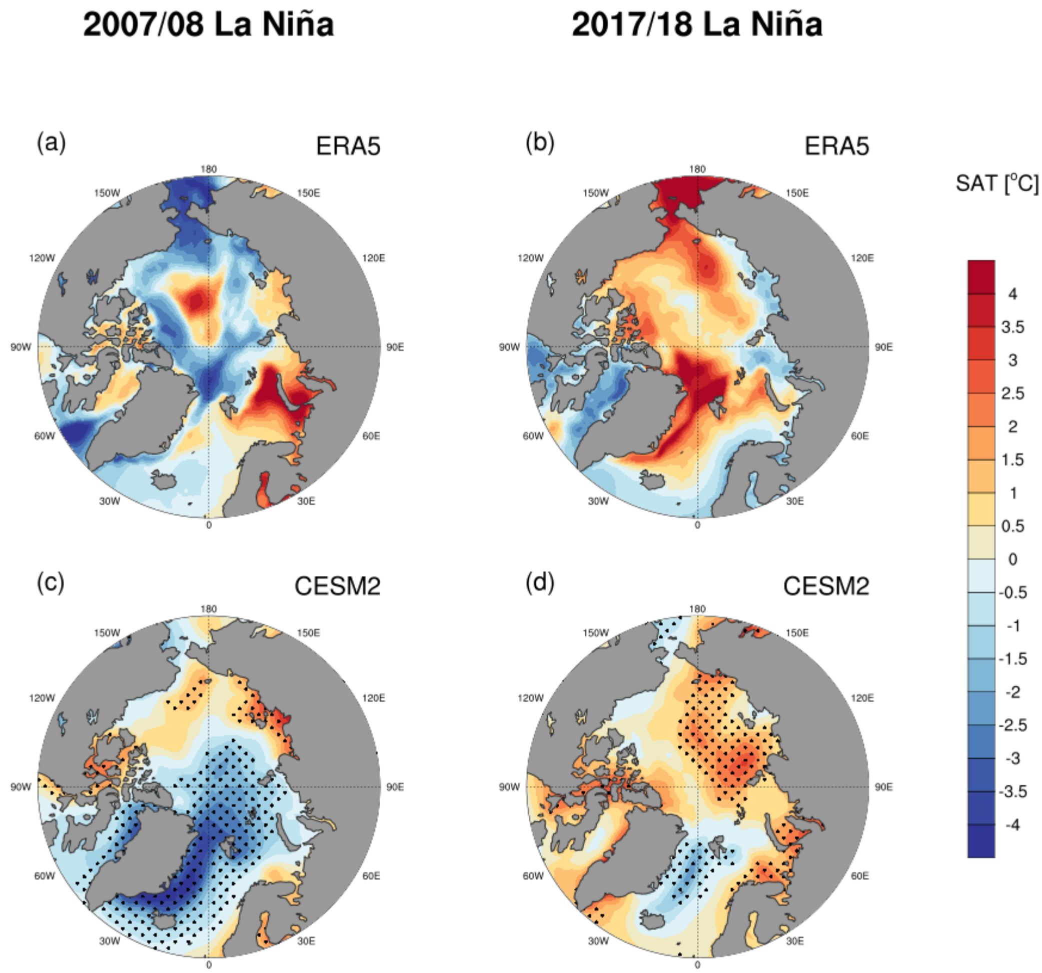

Fig. S8. Arctic SAT response during La Niña events. Surface air temperature (°C) anomalies over the Arctic Ocean in the winter (DJFM) for **(a, c)** 2007/08 and **(b, d)** 2017/18 from **(top)** ERA5 reanalysis and **(bottom)** CESM2 simulation. Statistically significant values ($p<0.05$) are stippled in **(c, d)**.

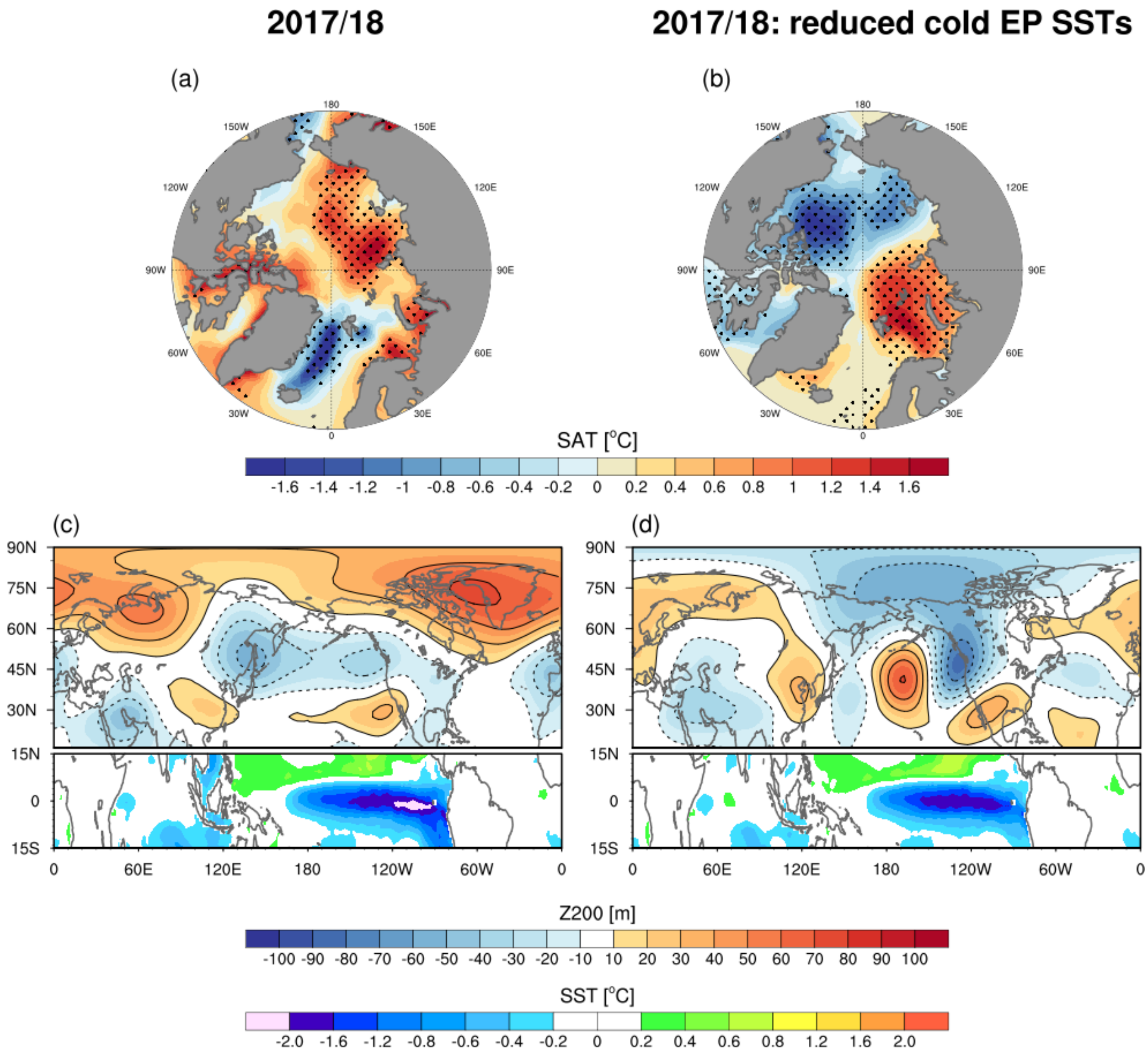

Fig. S9. Impacts of far-eastern equatorial Pacific SST anomalies on the Northern Hemisphere extratropics during the 2017/18 La Niña. (a, b) Surface air temperature (°C) anomalies over the Arctic Ocean and **(c, d)** extratropical (15°N-90°N) 200 hPa geopotential height anomalies (top panels; m) with tropical (15°S-15°N) SST anomalies (bottom panels; °C) in 2017/18 winter (DJFM) from **(a, c)** the original CESM2 pacemaker simulation and **(b, d)** 'iEP' simulation, in which the far equatorial eastern Pacific SST anomalies are increased. Statistically significant values ($p<0.05$) are stippled in **(a, b)**.

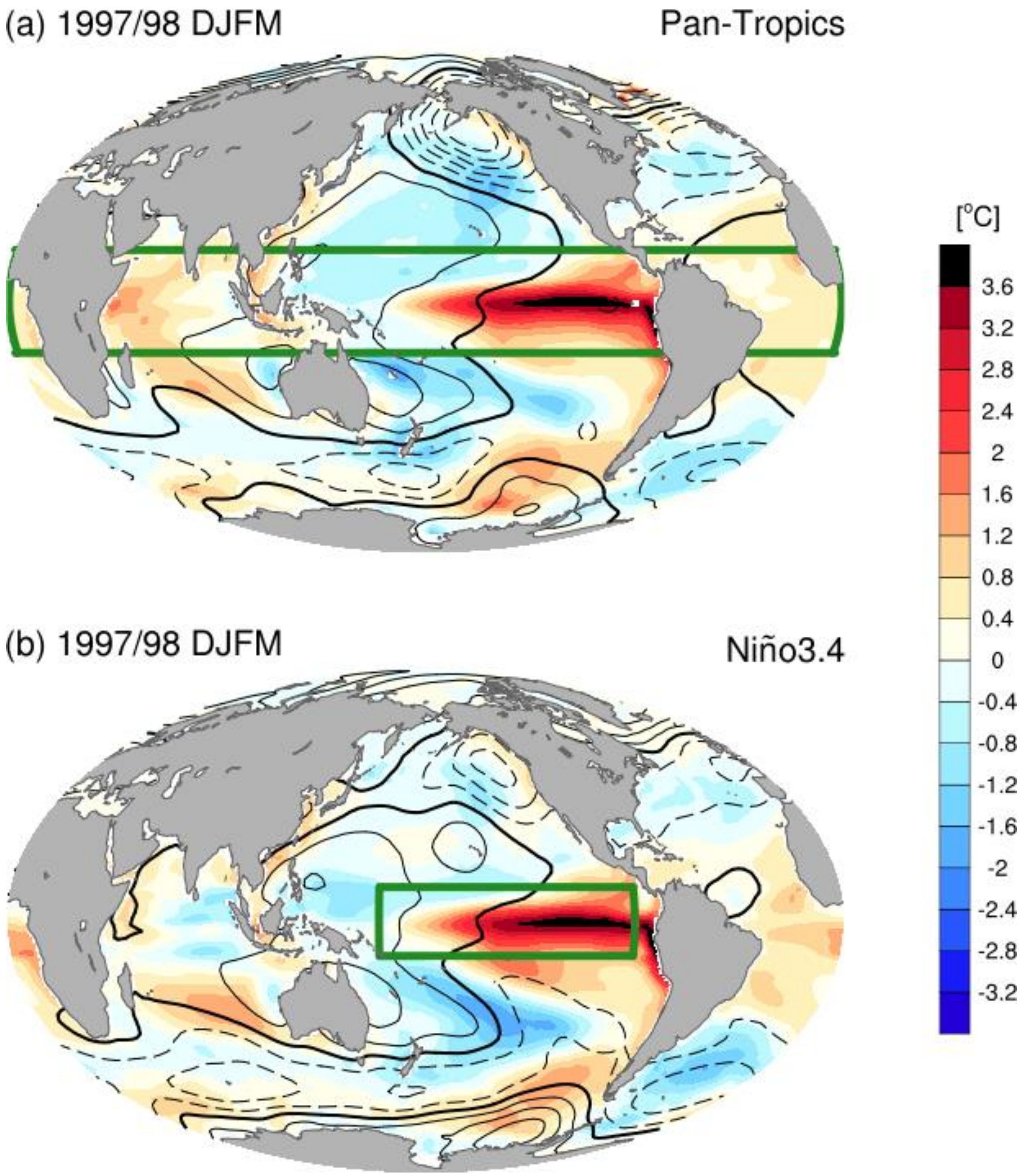

Fig. S10. The pacemaker region in the CESM2 simulation. SST (shading; °C) and SLP (contour; 2 hPa interval) anomalies during 1997/98 DJFM from the ensemble mean of the CESM2 pacemaker simulation over the **(a)** pan-tropics and **(b)** Niño3.4 region. The green boxes in **(a)** and **(b)** indicate the pacemaker region over 15°S – 15°N, 0 – 360°E and the Niño3.4 region over 10°S – 10°N, 160°E – 90°W, respectively.

Table S1. Time periods of CESM2 pacemaker simulations over Niño3.4. The two different periods of for each El Niño pacemaker simulation and the corresponding averaging periods for calculating the climatological-mean SSTs.

Experiments	Target SST	1982/83 El Niño	1997/98 El Niño
El Niño pacemaker simulations	Observed SSTs in the Niño3.4	1982.04 – 1983.03	1997.04 – 1998.03
Control simulation	Climatological-mean SSTs in the Niño3.4	Avg. (1981 – 1999)	Avg. (1986 – 2005)

Table S2. Idealized pacemaker simulations over pan-tropics. Idealized pacemaker experiments for 1997/98 El Niño

Experiments	cIO	dEP
El Niño pacemaker simulations	Observed SSTs in the deep tropics + Climatological SST over the Indian Ocean (1997.04 – 1998.03)	Observed SSTs in the deep tropics + Decreased SST over the equatorial Eastern Pacific (1997.04 – 1998.03)
Control simulation	Climatological-mean SSTs in the deep tropics (1986 – 2005)	Climatological-mean SSTs in the deep tropics (1986 – 2005)

Table S3. Idealized pacemaker simulation for the 2017/18 La Niña.

Experiments	iEP
La Niña pacemaker simulations	Observed SSTs in the deep tropics + Increased SST over the equatorial Eastern Pacific (2017.04 – 2018.03)
Control simulation	Climatological-mean SSTs in the deep tropics (2000 – 2018)

REFERENCES AND NOTES

1. J. A. Screen, C. Deser, D. M. Smith, X. Zhang, R. Blackport, P. J. Kushner, T. Oudar, K. E. McCusker, L. Sun, Consistency and discrepancy in the atmospheric response to Arctic sea-ice loss across climate models. *Nat. Geosci.* **11**, 155–163 (2018).

2. A. Dai, M. Song, Little influence of Arctic amplification on mid-latitude climate. *Nat. Clim. Chang.* **10**, 231–237 (2020).

3. J. Cohen, X. Zhang, J. Francis, T. Jung, R. Kwok, J. Overland, T. J. Ballinger, U. S. Bhatt, H. W. Chen, D. Coumou, S. Feldstein, H. Gu, D. Handorf, G. Henderson, M. Ionita, M. Kretschmer, F. Laliberte, S. Lee, H. W. Linderholm, W. Maslowski, Y. Peings, K. Pfeiffer, I. Rigor, T. Semmler, J. Stroeve, P. C. Taylor, S. Vavrus, T. Vihma, S. Wang, M. Wendisch, Y. Wu, J. Yoon, Divergent consensuses on Arctic amplification influence on midlatitude severe winter weather. *Nat. Clim. Chang.* **10**, 20–29 (2020).

4. H.-S. Park, S. Lee, Y. Kosaka, S.-W. Son, S.-W. Kim, The impact of Arctic winter infrared radiation on early summer sea ice. *J. Clim.* **28**, 6281–6296 (2015).

5. A. Letterly, J. Key, Y. Liu, The influence of winter cloud on summer sea ice in the Arctic, 1983–2013. *J. Geophys. Res.* **121**, 2178–2187 (2016).

6. B. M. Hegyi, P. C. Taylor, The unprecedented 2016–2017 Arctic sea ice growth season: The crucial role of atmospheric rivers and longwave fluxes. *Geophys. Res. Lett.* **45**, 5204–5212 (2018).

7. M. F. Stuecker, C. M. Bitz, K. C. Armour, C. Proistosescu, S. M. Kang, S.-P. Xie, D. Kim, S. M. Gregor, W. Zhang, S. Zhao, W. Cai, Y. Dong, F.-F. Jin, Polar amplification dominated by local forcing and feedbacks. *Nat. Clim. Chang.* **8**, 1076–1081 (2018).

8. H. Goosse, J. E. Kay, K. C. Armour, A. Bodas-Salcedo, H. Chepfer, D. Docquier, A. Jonko, P. J. Kushner, O. Lecomte, F. Massonnet, H.-S. Park, F. Pithan, G. Svensson, M. Vancoppenolle, Quantifying climate feedbacks in polar regions. *Nat. Commun.* **9**, 1919 (2018).

9. C. Stan, D. M. Straus, J. S. Frederiksen, H. Lin, E. D. Maloney, C. Schumacher, Review of tropical-extratropical teleconnections on intraseasonal time scales. *Rev. Geophys.* **55**, 902–937 (2017).

10. X. Yuan, M. R. Kaplan, M. A. Cane, The interconnected global climate system—A review of tropical–polar teleconnections. *J. Clim.* **31**, 5765–5792 (2018).

11. F. Sassi, D. Kinnison, B. A. Boville, R. R. Garcia, R. Roble, Effect of El Niño–Southern Oscillation on the dynamical, thermal, and chemical structure of the middle atmosphere. *J. Geophys. Res.*, **109**, D17108 (2004).

12. S. Lee, Testing of the tropically excited Arctic warming mechanism (TEAM) with traditional El Niño and La Niña. *J. Clim.* **25**, 4015–4022 (2012).

13. C. Hu, S. Yang, Q. Wu, Z. Li, J. Chen, K. Deng, T. Zhang, C. Zhang, Shifting El Niño inhibits summer Arctic warming and Arctic sea-ice melting over the Canada Basin. *Nat. Commun.* **7**, 11721 (2016).

14. M. R. McCrystall, J. A. Screen, Arctic winter temperature variations correlated With ENSO are dependent on coincidental sea ice changes. *Geophys. Res. Lett.* **48**, e2020GL091519 (2021).

15. R. Clancy, C. Bitz, E. Blanchard-Wrigglesworth, The influence of ENSO on Arctic sea ice in large ensembles and observations. *J. Clim.* **34**, 9585–9604 (2021).

16. N. C. Johnson, Y. Kosaka, The impact of eastern equatorial Pacific convection on the diversity of boreal winter El Niño teleconnection patterns. *Clim. Dyn.* **47**, 3737–3765 (2016).

17. N. K. Larkin, D. E. Harrison, Global seasonal temperature and precipitation anomalies during El Niño autumn and winter. *Geophys. Res. Lett.* **32**, L16705 (2005).

18. J.-S. Kug, F.-F. Jin, S.-I. An, Two types of El Niño events: Cold tongue El Niño and warm pool El Niño. *J. Clim.* **22**, 1499–1515 (2009).

19. H. Y. Kao, J.-Y. Yu, Contrasting eastern-pacific and central-pacific types of ENSO. *J. Clim.* **22**, 615–632 (2009).

20. Z. Li, W. Zhang, M. F. Stuecker, H. Xu, F.-F. Jin, C. Liu, Different effects of two ENSO types on Arctic surface temperature in boreal winter. *J. Clim.* **32**, 4943–4961 (2019).

21. H. Paek, J.-Y. Yu, C. Qian, Why were the 2015/2016 and 1997/1998 extreme El Niños different? *Geophys. Res. Lett.* **44**, 1848–1856 (2017).

22. L. Chen, T. Li, B. Wang, L. Wang, Formation mechanism for 2015/16 super El Niño. *Sci. Rep.* **7**, 2975 (2017).

23. M. L. L'Heureux, K. Takahashi, A. B. Watkins, A. G. Barnston, E. J. Becker, Tom E. Di Liberto, F. Gamble, J. Gottschalck, M. S. Halpert, B. Huang, K. Mosquera-Vásquez, A. T. Wittenberg, Observing and predicting the 2015/16 El Niño. *Bull. Am. Meteorol. Soc.* **98**, 1363–1382 (2017).

24. S. P. Xie, K. Hu, J. Hafner, H. Tokinaga, Y. Du, G. Huang, T. Sampe, Indian Ocean capacitor effect on Indo–western Pacific climate during the summer following El Niño. *J. Clim.*, **22**, 730–747 (2009).

25. W. Zhang, Y. Wang, F.-F. Jin, M. F. Stuecker, A. G. Turner, Impact of different El Niño types on the El Niño/IOD relationship. *Geophys. Res. Lett.* **42**, 8570–8576 (2015).

26. S. Yang, Z. Li, J.-Y. Yu, X. Hu, W. Dong, S. He, El Niño-Southern Oscillation and its impact in the changing climate. *Natl. Sci. Rev.* **5**, 840–857 (2018).

27. N. H. Saji, B. N. Goswami, P. N. Vinayachandran, T. Yamagata, A dipole mode in the tropical Indian Ocean. *Nature* **401**, 360–363 (1999).

28. N. J. Abram, N. M. Wright, B. Ellis, B. C. Dixon, J. B. Wurtzel, M. H. England, C. C. Ummenhofer, B. Philibosian, S. Y. Cahyarini, T.-L. Yu, C.-C. Shen, H. Cheng, R. L. Edwards, D. Heslop, Coupling of Indo-Pacific climate variability over the last millennium. *Nature* **579**, 385–392 (2020).

29. M. F. Stuecker, C. M. Bitz, K. C. Armour, Conditions leading to the unprecedented low Antarctic sea ice extent during the 2016 austral spring season. *Geophys. Res. Lett.* **44**, 9008–9019 (2017).

30. S. W. Yeh, W. Cai, S. K. Min, M. J. McPhaden, D. Dommenget, B. Dewitte, M. Collins, K. Ashok, S. I. An, B. Y. Yim, J. S. Kug, ENSO atmospheric teleconnections and their response to greenhouse gas forcing. *Rev. Geophys.* **56**, 185–206 (2018).

31. J. C. Comiso, Warming trends in the Arctic from clear sky satellite observations. *J. Clim.* **16**, 3498–3510 (2003).

32. C. Deser, I. R. Simpson, K. A. McKinnon, A. S. Phillips, The Northern Hemisphere extratropical atmospheric circulation response to ENSO: How well do we know it and how do we evaluate models accordingly? *J. Clim.* **30**, 5059–5082 (2017).

33. N. Soulard, H. Lin, B. Yu, The changing relationship between ENSO and its extratropical response patterns. *Sci. Rep.* **9**, 6507 (2019).

34. R. Chen, I. R. Simpson, C. Deser, B. Wang, Model biases in the simulation of the springtime North Pacific ENSO teleconnection. *J. Clim.*, **33**, 9985–10002 (2020).

35. K. Park, S. M. Kang, D. Kim, M. F. Stuecker, F. F. Jin, Contrasting local and remote impacts of surface heating on polar warming and amplification. *J. Clim.*, **31**, 3155–3166 (2018).

36. S. He, X. Xu, T. Furevik, Y. Gao, Eurasian cooling linked to the vertical distribution of Arctic warming. *Geophys. Res. Lett.* **47**, e2020GL087212 (2020).

37. Q. Ding, J. M. Wallace, D. S. Battisti, E. J. Steig, A. J. Gallant, H. J. Kim, L. Geng, Tropical forcing of the recent rapid Arctic warming in northeastern Canada and Greenland. *Nature* **509**, 209–212 (2014).

38. R. A. Plumb, On the three-dimensional propagation of stationary waves. *J. Atmos. Sci.* **42**, 217–229 (1985).

39. S. Hu, A. V. Fedorov, Indian Ocean warming as a driver of the North Atlantic warming hole. *Nat. Commun.* **11**, 4785 (2020).

40. A. S. Taschetto, R. R. Rodrigues, G. A. Meehl, S. McGregor, M. H. England, How sensitive are the Pacific–tropical North Atlantic teleconnections to the position and intensity of El Niño-related warming? *Clim. Dyn.* **46**, 1841–1860 (2016).

41. Z. Q. Zhou, S. P. Xie, X. T. Zheng, Q. Liu, H. Wang, Global warming-induced changes in El Niño teleconnections over the North Pacific and North America. *J. Clim.* **27**, 9050–9064 (2014).

42. S. Matsumura, K. Yamazaki, T. Horinouchi, Robust asymmetry of the future Arctic polar vortex is driven by tropical Pacific warming. *Geophys. Res. Lett.* **48**, e2021GL093440 (2021).

43. M. Goss, S. B. Feldstein, S. Lee, Stationary wave interference and its relation to tropical convection and Arctic warming. *J. Clim.*, **29**, 1369–1389 (2016).

44. V. E. Larson, CLUBB-SILHS: A parameterization of subgrid variability in the atmosphere. arXiv:1711.03675 [physics.ao-ph] (2017).

5. R. Smith, P. Jones, B. Briegleb, F. Bryan, G. Danabasoglu, J. Dennis, J. Dukowicz, *C. Eden*, B. Fox-Kemper, P. Gent, M. Hecht, "The Parallel Ocean Program (POP) reference manual: Ocean component of the Community Climate System Model (CCSM)" (Technical Report, Los Alamos National Laboratory, 2010).

46. D. M. Lawrence, R. A. Fisher, C. D. Koven, K. W. Oleson, S. C. Swenson, G. Bonan, N. Collier, B. Ghimire, L. van Kampenhout, D. Kennedy, E. Kluzek, P. J. Lawrence, F. Li, H. Li, D. Lombardozzi, W. J. Riley, W. J. Sacks, M. Shi, M. Vertenstein, W. R. Wieder, C. Xu, A. A. Ali, A. M. Badger, G. Bisht, M. van den Broeke, M. A. Brunke, S. P. Burns, J. Buzan, M. Clark, A. Craig, K. Dahlin, B. Drewniak, J. B. Fisher, M. Flanner, A. M. Fox, P. Gentine, F. Hoffman, G. Keppel-Aleks, R. Knox, S. Kumar, J. Lenaerts, L. R. Leung, W. H. Lipscomb, Y. Lu, A. Pandey, J. D. Pelletier, J. Perket, J. T. Randerson, D. M. Ricciuto, B. M. Sanderson, A. Slater, Z. M. Subin, J. Tang, R. Quinn Thomas, M. V. Martin, X. Zeng, The community land model version 5: Description of new features, benchmarking, and impact of forcing uncertainty. *J. Adv. Model. Earth Syst.* **11**, 4245–4287 (2019).

47. E. C. Hunke, W. H. Lipscomb, A. K. Turner, N. Jeffery, S. Elliott, "CICE: The Los Alamos Sea Ice Model Documentation and Software User's Manual Version 5.1" (Technical Report no. LA-CC-06-012, Los Alamos National Laboratory, 2015).

48. R. W. Reynolds, N. A. Rayner, T. M. Smith, D. C. Stokes, W. Wang, An improved in situ and satellite SST analysis for climate. *J. Clim.* **15**, 1609–1625 (2002).

49. H. Hersbach, B. Bell, P. Berrisford, S. Hirahara, A. Horányi, J. Muñoz-Sabater, J. Nicolas, C. Peubey, R. Radu, D. Schepers, A. Simmons, C. Soci, S. Abdalla, X. Abellan, G. Balsamo, P. Bechtold, G. Biavati, J. Bidlot, M. Bonavita, G. De Chiara, P. Dahlgren, D. Dee, M. Diamantakis, R. Dragani, J. Flemming, R. Forbes, M. Fuentes, A. Geer, L. Haimberger, S. Healy, R. J. Hogan, E. Hólm, M. Janisková, S. Keeley, P. Laloyaux, P. Lopez, C. Lupu, G. Radnoti, P. de Rosnay, I. Rozum, F. Vamborg, S. Villaume, J.-N. Thépaut, The ERA5 global reanalysis. *Q. J. R. Meteorol. Soc.* **146**, 1999–2049 (2020).

50. F. Fetterer, K. Knowles, W. N. Meier, M. Savoie, A. K. Windnagel, Sea ice index, version 3 (National Snow and Ice Data Center, 2017).

51. P. C. Austin, J. V. Tu, Bootstrap methods for developing predictive models. *Am. Stat.* **58**, 131–137 (2004).

52. M. Yanai, S. Esbensen, J.-H. Chu, Determination of bulk properties of tropical cloud clusters from large-scale heat and moisture budgets. *J. Atmos. Sci.* **30**, 611–627 (1973).

53. P. C. Hsu, T. Li, Interactions between boreal summer intraseasonal oscillations and synoptic-scale disturbances over the western North Pacific. Part II: Apparent heat and moisture sources and eddy momentum transport*. *J. Clim.* **24**, 942–961 (2011).

54. S. Lee, T. Gong, N. Johnson, S. B. Feldstein, D. Pollard, On the possible link between tropical convection and the Northern Hemisphere Arctic surface air temperature change between 1958 and 2001. *J. Clim.*, **24**, 4350–4367 (2011).